Human Molecular Genetics, 2012, Vol. 21, No. 24 **5294–5305**
doi:10.1093/hmg/dds380
Advance Access published on September 13, 2012

Pantothenate kinase-associated neurodegeneration: altered mitochondria membrane potential and defective respiration in *Pank2 knock-out* mouse model

Dario Brunetti[1], Sabrina Dusi[1], Michela Morbin[2], Andrea Uggetti[2], Fabio Moda[2], Ilaria D'Amato[1], Carla Giordano[3], Giulia d'Amati[3], Anna Cozzi[4], Sonia Levi[4,5], Susan Hayflick[6,7,8] and Valeria Tiranti[1,*]

[1]Unit of Molecular Neurogenetics and [2]Unit of Neurology and Neuropathology, IRCCS Foundation Neurological Institute 'C. Besta', Milan, Italy [3]Department of Radiological, Oncological and Pathological Sciences, Sapienza University, Policlinico Umberto I, Rome, Italy, [4]San Raffaele Scientific Institute and [5]Division of Neuroscience, Vita-Salute San Raffaele University, Milan, Italy and [6]Department of Molecular and Medical Genetics, [7]Department of Pediatrics and [8]Department of Neurology, Oregon Health & Science University, Portland, OR, USA

Received August 9, 2012; Revised and Accepted September 5, 2012

Neurodegeneration with brain iron accumulation (NBIA) comprises a group of neurodegenerative disorders characterized by high brain content of iron and presence of axonal spheroids. Mutations in the *PANK2* gene, which encodes pantothenate kinase 2, underlie an autosomal recessive inborn error of coenzyme A metabolism, called pantothenate kinase-associated neurodegeneration (PKAN). PKAN is characterized by dystonia, dysarthria, rigidity and pigmentary retinal degeneration. The pathogenesis of this disorder is poorly understood and, although PANK2 is a mitochondrial protein, perturbations in mitochondrial bioenergetics have not been reported. A knock-out (KO) mouse model of PKAN exhibits retinal degeneration and azoospermia, but lacks any neurological phenotype. The absence of a clinical phenotype has partially been explained by the different cellular localization of the human and murine PANK2 proteins. Here we demonstrate that the mouse Pank2 protein localizes to mitochondria, similar to its human orthologue. Moreover, we show that Pank2-defective neurons derived from KO mice have an altered mitochondrial membrane potential, a defect further corroborated by the observations of swollen mitochondria at the ultra-structural level and by the presence of defective respiration.

INTRODUCTION

Pantothenate kinase-associated neurodegeneration (PKAN) is the main disorder of a nosological family termed neurodegeneration with brain iron accumulation (NBIA), in which accumulated iron can be visualized by radiological and histopathological examination of the brain. PKAN is an autosomal-recessive disorder characterized by progressive motor impairment, associated with profound dystonia due to mutations in the *PANK2* gene. This gene codes for a mitochondrial enzyme involved in the first regulatory step of coenzyme A (CoA). CoA is synthesized from vitamin B5, or pantothenate, and plays key roles in basic cellular functions such as fatty acid metabolism, Krebs cycle and amino acid synthesis. Pantothenate is taken up by endothelial cells via a sodium-dependent multivitamin transporter and then passes to the blood for delivery to the rest of the body (1). Pantothenate is phosphorylated by pantothenate kinase, conjugated to cysteine, decarboxylated, conjugated to an adenosyl group and phosphorylated again to form CoA. These enzymatic activities

*To whom correspondence should be addressed at: Unit of Molecular Neurogenetics, IRCCS Foundation Neurological Institute 'C. Besta', Via Temolo, 4, 20126 Milan, Italy. Tel: +39 0223942633; Fax: +39 0223942619; Email: tiranti@istituto-besta.it

have been detected in the cytosol and many in the mitochondrion, as well. An exclusively mitochondrial CoA synthetic pathway has been proposed (2,3), although the cysteine ligase and decarboxylation activities have not been detected explicitly in the mitochondrion. PANK1, PANK2, PANK3 and PANK4 are four known isoforms of pantothenate kinase. Probably PANK4 is not functional as pantothenate kinase, but PANK1 and PANK3 are active in the cytosol, while PANK2 is localized to and active in the mitochondrion (4).

The study of PANK2 function is complex, and efforts to generate animal models of disease by knocking out the gene in flies and mice have generated incomplete phenotypes, lacking signs of neurodegeneration and/or of brain iron accumulation (5,6). A PKAN model of *Drosophila* has a brain phenotype characterized by the formation of vacuoles, absence of iron accumulation, and *Drosophila* pantothenate kinase isoforms do not strictly parallel those of humans (5). In 2005, *Pank2* null mice were generated (7), which showed growth reduction, retinal degeneration and male infertility due to azoospermia but no movement disorder or brain iron accumulation, even after 18 months of age. In contrast, a pantothenic acid-deficient diet was able to elicit a movement disorder and azoospermia in mice without evidence of iron accumulation in brain (8).

These results have partially been explained by the subcellular localization of the murine Pank2 protein, which was reported to be predominately mitochondrial (9) or cytoplasmic (10) by different groups. We performed experiments aimed at demonstrating: (i) the sub-cellular localization of the murine Pank2 protein and (ii) the presence of alterations in the function, regulation and structure of mitochondria in the available KO mouse model. Our studies have demonstrated that *Pank2* KO mice have mitochondrial dysfunction.

RESULTS

Mitochondrial localization of mouse Pank2 protein

Human and mouse PANK2 proteins show an identity of 90%, although the mouse polypeptide does not have an N-terminal extension, which is present in human PANK2. Software tools predicting mitochondrial localization of proteins scored high for the murine Pank2: Mitoprot (http://ihg.gsf.de/ihg/mitoprot.html) gave a probability of 98%; Predotar (http://urgi.versailles.inra.fr/predotar/predotar.html) of 72%, and TargetP (http://www.cbs.dtu.dk/services/TargetP/) of 88%. To experimentally verify the sub-cellular localization of the murine protein, we performed western blot analysis using a commercially available antibody (see Material and Methods) on total homogenate, cytosol and mitochondria isolated from brain and fibroblasts of wild-type (WT; $Pank2^{+/+}$) and knock-out (KO; $Pank2^{-/-}$) mice. We first tested specificity of the antibody by verifying its cross-reactivity with the Pank2 *in vitro* translation product (not shown).

In the homogenate and cytosol derived from $Pank2^{+/+}$ but not from $Pank2^{-/-}$ brain, the antibody detected a faint band of around 47 kDa, corresponding to the predicted molecular weight of the murine Pank2 protein (Fig. 1A). A band of higher intensity was present in mitochondria isolated from $Pank2^{+/+}$ mice, while it was completely absent in mitochondria derived from $Pank2^{-/-}$ mice. These data indicated that the Pank2 protein, which was detectable and enriched in the mitochondrial fraction of wild-type mice, was missing in $Pank2^{-/-}$ mice. To further determine in which submitochondrial compartment the Pank2 protein was present, we further fractionated mitochondria derived from WT mouse brain, into membranes, inter-membrane space, and matrix, and we isolated mitoplasts. As shown in Figure 1B, western blot analysis demonstrated that the mouse Pank2 protein was present into the mitochondrial inter-membrane space and mitoplasts. However, by exposing mitoplasts to the action of proteinase K (PK), the signal corresponding to the Pank2 protein disappeared. On the contrary, signals corresponding to proteins present in the mitochondrial matrix such as Ethe1, or in the inner membrane such as Ndufa9 remained protected from PK degradation. We obtained the same results by fractionating mitochondria derived from mouse fibroblasts (Fig. 1C). Altogether these data indicated that the mouse Pank2 protein could be mainly located in the mitochondrial inter-membrane space. In the mouse brain but not in fibroblasts, the protein was also barely detectable in the mitochondrial matrix.

Mitochondrial bioenergetics evaluation

In order to investigate mitochondrial bioenergetic status, we performed spectrophotometric assays to measure the biochemical activity of each single respiratory chain complex in different tissue homogenates (muscle, brain and liver) derived from $Pank2^{+/+}$ and $Pank2^{-/-}$ mice. No alterations in the specific activities of complex I, II, III, IV and V were observed (data not shown).

We then evaluated respiration with microscale oxygraphy on mitochondria isolated from mouse brain. This system measures global oxygen consumption rate (OCR) and extracellular acidification rate in intact cells and isolated mitochondria.

According to Brand and Nicholls (11), and our group (12) in intact cells, and by Rogers *et al*. (13) in isolated mitochondria, the direct readout of cellular respiration can be used to define relevant bioenergetic parameters, including (a) basal OCR (OCR-B), after ADP addition (OCR-ADP), after oligomycin addition (OCR-O).

We performed oxygen consumption measurement in three different $Pank2^{+/+}$ and $Pank2^{-/-}$ mice of 4 weeks of age. In each experiment, we consistently observed reductions of OCR-B, -ADP, −O, in mitochondria isolated from $Pank2^{-/-}$ brain when compared with $Pank2^{+/+}$ (Fig. 2A).

In another set of experiments, we also added FCCP (OCR-F) to measure uncoupler-stimulated respiration.

To compare the numerical results of the different experiments, individual values were used to obtain *z*-scores of OCR-B, -ADP, -O, -F (12).

For statistical analysis, we compared the *z*-scores obtained in the $Pank2^{+/+}$ versus $Pank2^{-/-}$ mitochondria (Fig. 2B). The values obtained in the WT mitochondria were consistently and significantly higher than those obtained in $Pank2^{-/-}$ mitochondria, for each of the mitochondrial respiratory conditions.

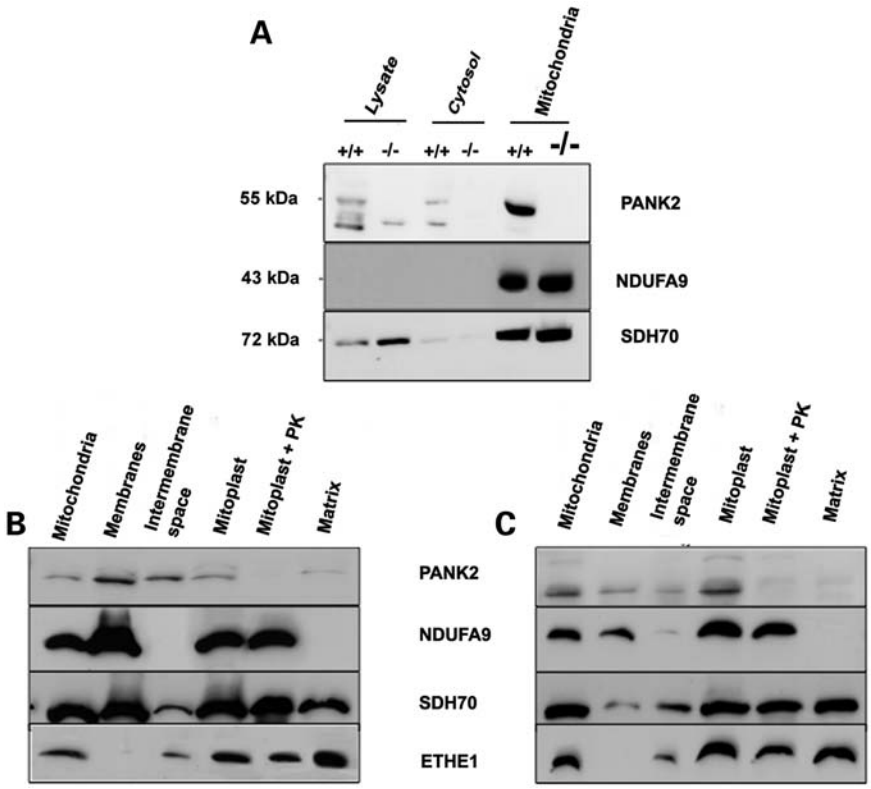

Figure 1. Mitochondrial localization of murine Pank2 protein. (**A**) Western blot analysis of different sub-cellular fractions derived from mouse brain: +/+ indicates *Pank2*$^{+/+}$ animals; −/− indicates *Pank2*$^{-/-}$ animals. The same filter was incubated with anti-PANK2, anti-NDUFA9 and anti-SDH70 antibodies. (**B**) Western blot analysis on different mitochondrial compartments isolated from WT mouse brain. (**C**) Western blot analysis on different mitochondrial compartments isolated from WT mouse fibroblasts. In (B and C) the filters were sequentially incubated with anti-PANK2, anti-NDUFA9, anti-SDH70 and anti-ETHE1 antibodies.

These differences were statistically significant as demonstrated by an unpaired, two-sided Student's *t*-test, assuming unequal variance. Values for statistical significance were set at $P < 0.05$.

We also evaluated the ATP content in cells derived from three *Pank2*$^{+/+}$ and three *Pank2*$^{-/-}$ mice.

We observed a reduced level of ATP in *Pank2*$^{-/-}$ derived cells when compared with *Pank2*$^{+/+}$ (Supplementary Material, Fig. S1A), suggesting a lower capacity to produce ATP in the absence of Pank2 protein. These data are in agreement with the observation of a global reduction of the respiratory capacity of intact mitochondria derived from *Pank2*$^{-/-}$ brains.

Parameters of oxidative stress

We measured the levels of protein carbonyl groups, a marker of protein oxidation, by OxyBlot assay in the brain of three *Pank2*$^{+/+}$ and three *Pank2*$^{-/-}$ mice of 6 months of age. The total level of carbonyls is similar between the two genotypic groups (Supplementary Material, Fig. S1B), although a certain level of variability was noticed. We also performed western blot analysis on the same samples with antibodies specific to superoxide dismutase 1 and Catalase, but again no significant differences were identified (not shown).

Mitochondrial morphology and integrity in peripheral and central nervous systems

Since PKAN affects the central nervous system (CNS) in humans, we sought to examine CNS neurons in mouse for evidence of perturbed mitochondrial structure or function. We derived neural precursors from hair bulge whisker (Supplementary Material, Fig. S2A) and sciatic nerve (Supplementary Material, Fig. S2B) of *Pank2*$^{-/-}$ and *Pank2*$^{+/+}$ mice and subsequently differentiated these cells into neurons (see Materials and Methods). Cells showed typical morphology of neural crest precursor (Supplementary Material, Fig. S2A), stained positive for neural crest marker Nestin (Supplementary Material, Fig. S2C and D) and were negative for glial fibrillary acidic protein staining (Supplementary Material, Fig. S2E and F). After induction with suitable culture medium, differentiated neurons (Supplementary Material, Fig. S2G and H) expressing the neuron-specific marker β-III-tubulin (Supplementary Material, Fig. S2I–L) were obtained. The Mitotracker red, a mitochondrion specific dye, was used to stain both hair bulge- and sciatic nerve-derived neurons obtained from *Pank2*$^{+/+}$ and *Pank2*$^{-/-}$ mice. We observed that the dye was exclusively localized into mitochondria in *Pank2*$^{+/+}$ neurons (Fig. 3A–C) while it was diffused throughout the cytoplasm and nucleus in *Pank2*$^{-/-}$ neurons (Fig. 3B–D).

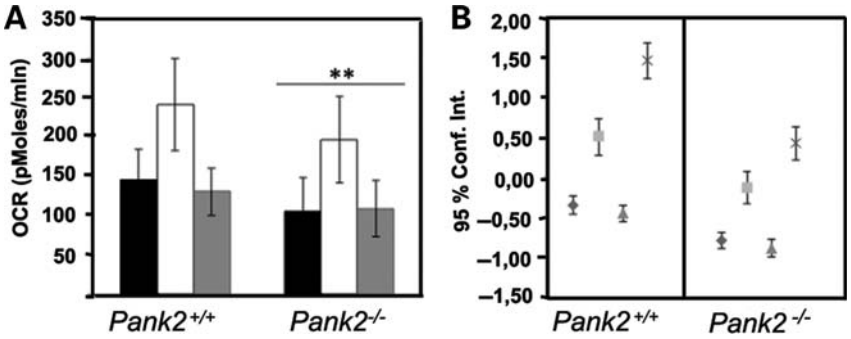

Figure 2. Evaluation of mitochondrial bioenergetics status. (**A**) OCR in *Pank2*$^{+/+}$ and *Pank2*$^{-/-}$ mouse brain mitochondria. Black, white and grey histograms indicate OCR-B, -ADP and -O, respectively. Bars indicate the standard deviation (SD). $^{**}P < 0.01$ (unpaired, two-tail Student's *t*-test). (**B**) Analysis of OCR-B, -ADP, -O and -F. The *z*-score values (dots) for OCR-B, -ADP, -O and -F are shown for *Pank2*$^{+/+}$ versus *Pank2*$^{-/-}$. Data are expressed as the means (dots) and 95% confidence intervals, Confidence interval (bars). Student's *t*-test for *Pank2*$^{+/+}$ versus *Pank2*$^{-/-}$: diamond, $P = 1.0E-07$; square, $P = 1.3E-04$; triangle, $P = 1.0E-07$; asterisk, $P = 1.2E-09$. Three *Pank2*$^{+/+}$ and three *Pank2*$^{-/-}$ mice of 4-week-old were analysed.

This difference was quantified by selecting a defined area corresponding to nucleus of neurons and by calculating the imageJ parameter 'RawIntDen' (that is the sum of the values of the pixels in the selected area) in WT and KO neurons. This parameter resulted in a 2.5-fold greater value in *Pank2*$^{-/-}$ neurons when compared with *Pank2*$^{+/+}$ neurons (Fig. 3G).

We reasoned that the type of Mitotracker used for the staining was also able to detect a qualitative defect in the mitochondrial membrane potential ($\Delta\Psi_m$) (14).

To verify these data, we treated control fibroblasts with the uncoupling agent valinomycin to induce the $\Delta\Psi_m$ loss. We observed that the Mitotracker stains mitochondria in untreated cells (Fig. 3E), while it spreads in the cytoplasm in fibroblasts exposed to valinomycin (Fig. 3F).

To further corroborate these data we used 5,5′,6,6′-tetrachloro-1,1′,3,3′ tetraethylbenzimidazolylcarbocyanine iodide (JC1) staining, which specifically detects variation in the mitochondrial membrane potential. The JC1 dye undergoes a reversible change in fluorescence emission from green to red as mitochondrial membrane potential increases. Cells with high membrane potential promote the formation of red fluorescent aggregates, while cells with low membrane potential show a diffuse green fluorescence. As shown in Figure 4A, C, E, WT neurons of different derivation presented red fluorescent aggregates, while KO neurons presented predominantly with a diffuse green fluorescence (Fig. 4B–F). JC1 specificity was tested by pre-treating WT neurons with valinomycin. As reported in Supplementary Material, Figure S3, treated neurons stain green fluorescent aggregates, whereas untreated neurons showed red fluorescent aggregates.

To corroborate our observations, we performed electron microscopic analysis on neurons in culture, which were stained with JC1. Examination of semi-thin sections revealed the presence of enlarged neurons with severe alteration in the cytoplasm, containing abundant micro-vesicular structures, mainly if not exclusively in *Pank2*$^{-/-}$ cells (Fig. 4H). Ultrastructural investigation confirmed that, while the cytoplasm of *Pank2*$^{+/+}$ neurons exclusively showed endoplasmic reticulum, vesicles and mitochondria with regular morphology (Fig. 4I–K), *Pank2*$^{-/-}$ neurons contained lipid droplets, and several swollen mitochondria with aberrant cristae and a complete alteration of the matrix structure (Fig. 4J–L), together with morphologically normal mitochondria.

We asked whether the same alteration observed in the peripheral nerve and neurons was also present in the CNS of *Pank2*$^{-/-}$ mice. To this aim, we derived neonatal hippocampal neonatal neurons and we performed the JC1 staining experiment. As reported in Figure 4E, a red fluorescent signal was detected in neurons derived from *Pank2*$^{+/+}$ mice, whereas a green fluorescent signal (Fig. 4F) was exclusively present in neurons derived from *Pank2*$^{-/-}$ animals.

Altogether, these data demonstrated that aberrant mitochondria were present not only in neurons derived from the sciatic nerve of adult animals, but also in neonatal hippocampal neurons.

Analysis of peripheral and CNSs

We analysed the sciatic nerve obtained from groups of three *Pank2*$^{+/+}$ and three *Pank2*$^{-/-}$ animals of 24 and 48 weeks of age, respectively.

Examination of semithin sections, counterstained with Toluidine Blue, revealed no obvious differences in myelinated fibre density, in the absence of demyelinating features. However, *Pank2*$^{-/-}$ nerve showed a mild reduction in large-caliber fibre and some more prominent wallerian-like degenerations compared with controls (Fig. 5A and B). Overall, no clear-cut sign of progressive neuropathy was present, since no reduction in myelinated fibres or increase in the number of degenerating fibres has been detected (Fig. 5C and D).

Ultra-structural analysis of sciatic nerve of *Pank2*$^{-/-}$ animals confirmed the presence of occasional degenerating fibres, and a normal representation of un-myelinated fibres (Fig. 5E and F). However, a substantial number of myelinated fibres (Fig. 6B–D), and occasionally un-myelinated axons and Schwann cells, contained (Supplementary Material, Fig. S4B–D) swollen mitochondria, characterized by alteration of cristae and by the presence of multivesicolar bodies or amorphous material, in the matrix (Fig. 6A–C and Supplementary Material, Fig. S4A–C). Aberrant mitochondria appear to increase with age since in 48 week *Pank2*$^{-/-}$ old mice versus 24 week old mice (Fig. 6B) a greater number of swollen mitochondria with a profound alteration of the matrix were detected (Fig. 6D).

We also analysed the basal ganglia of 48-week-old mice. Electron microscopy demonstrated morphologically abnormal mitochondrial cristae with enlarged cisternae, which were

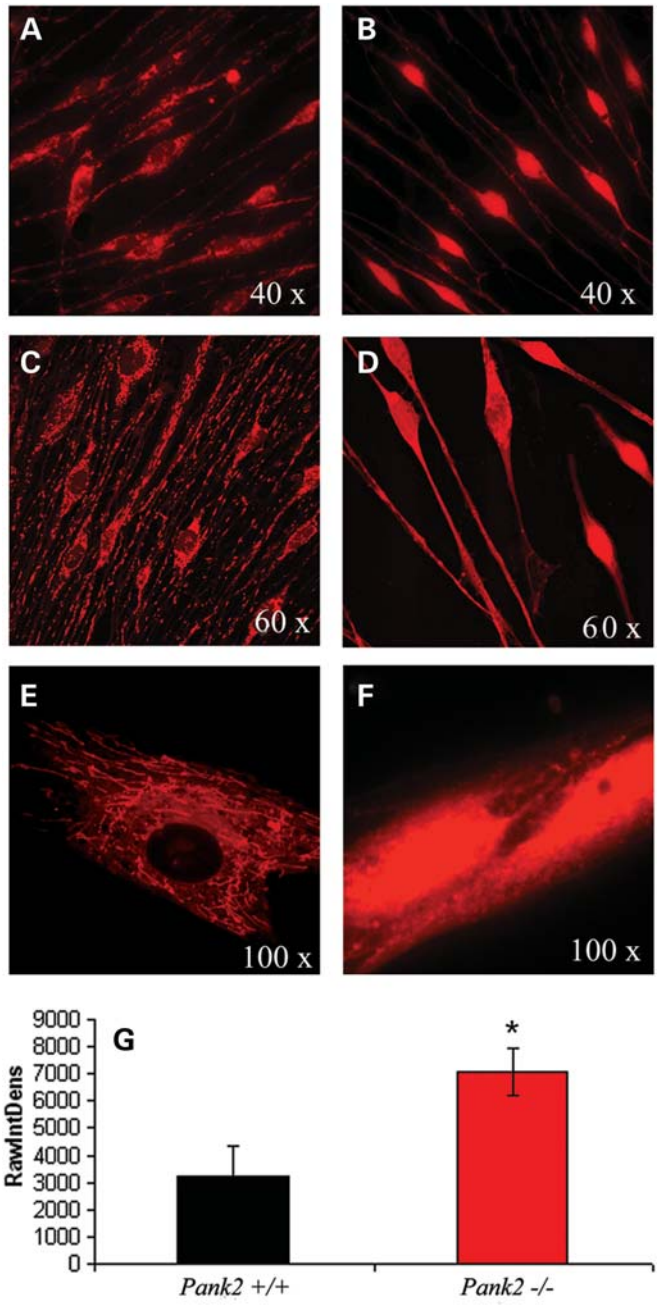

Figure 3. Mitochondrial morphology evaluated with the Mitotracker-red. (**A**) Neurons derived from hair bulge from *Pank2*$^{+/+}$ mice. (**B**) Neurons derived from hair bulge from *Pank2*$^{-/-}$ mice. (**C**) Neurons derived from sciatic nerve of *Pank2*$^{+/+}$ mice. (**D**) Neurons derived from sciatic nerve of *Pank2*$^{-/-}$ mice. (**E**) Control fibroblasts. (**F**) Control fibroblasts treated with valinomycin. (**G**) Histogram reporting the quantification of Mitotracker diffusion in *Pank2*$^{+/+}$ and *Pank2*$^{-/-}$ neurons using the RawIntDen parameter (see Materials and Methods). Bars indicated SD. $^{*}P = 3.37\text{E}-23$ (unpaired, two-tail Student's *t*-test).

predominant in the *Pank2*$^{-/-}$ (Fig. 6F–H) when compared with *Pank2*$^{+/+}$ (Fig. 6E–G).

These data indicate the presence of defective mitochondria in both the peripheral and CNSs in mice with defective *Pank2*.

DISCUSSION

We have demonstrated that the murine Pank2 protein is mainly located in the mitochondrial inter-membrane space, which is compatible with its role in CoA metabolism and with its regulation in the presence of CoA at concentrations found in mitochondrial matrix (10). Further investigation using, for instance, immuno-electronmicroscopy is needed to unequivocally establish this sub-mitochondrial localization.

This observation makes the *Pank2*$^{-/-}$ mouse model a promising system to study pathophysiology of human PKAN. In fact, although the mouse model does not recapitulate the clinical and neuropathological features of the human condition (7), it could serve as a system in which to interrogate the basic defect in mitochondrial function.

We did not detect the deficiency in the enzymatic activity of any mitochondrial respiratory chain complex in different tissues of *Pank2*$^{-/-}$ mice. However, recent observations indicate that mitochondrial respiration is largely carried out by the fraction of respiratory chain complexes that assemble together in supercomplexes forming functionally active units, called respirasomes (15,16). Thus, the spectrophotometric measurement of each respiratory complex activity does not necessarily reflect the mitochondrial functional capacity *in vivo*. Microscale oxygraphy could overcome this limitation and in fact, using this approach, we detected a modification in the respiratory profile of mitochondria derived from *Pank2*$^{-/-}$ when compared with *Pank2*$^{+/+}$ brains. Highly significant differences of OCR-B, -ADP, -O and –F were obtained by statistical analysis of either the single values or as overall values of *Pank2*$^{+/+}$ versus *Pank2*$^{-/-}$ mitochondria, expressed as *z*-scores (Fig. 2). Together, these results indicate that the absence of the Pank2 protein leads to a global failure of the mitochondrial bioenergetic performance without affecting the function of any single respiratory chain complex.

An interesting result of our study, strictly correlated with the absence of Pank2 function, was the demonstration of alteration in mitochondrial membrane potential in neurons derived from sciatic nerve and hair bulge stem cells of adult mice. In addition, the same alteration was also present in neonatal hippocampal neurons, suggesting the presence of defective mitochondria in *Pank2*$^{-/-}$ mice since birth.

These results were confirmed by electron microscopy analysis on cultured neurons derived from *Pank2*$^{-/-}$ mice, in which aberrant mitochondria with remodelled cristae were present. Moreover, peripheral and CNSs examination of *Pank2*$^{-/-}$ mice showed the presence of swollen mitochondria with amorphous electron-dense inclusions and dysmorphic cristae.

Recently, the characterization of a PKAN *Drosophila* model demonstrated that impaired function of pantothenate kinase induced a neurodegenerative phenotype with mitochondrial dysfunction, decreased levels of CoA, increased protein oxidation and reduced lifespan (17).

JC1 staining and electron microscopic analysis revealed that, in contrast to WT flies, mitochondria of dPANK/fbl mutants showed an alteration in the transmembrane potential, were swollen and presented with altered cristae and ruptured membranes (18). These observations are in agreement with

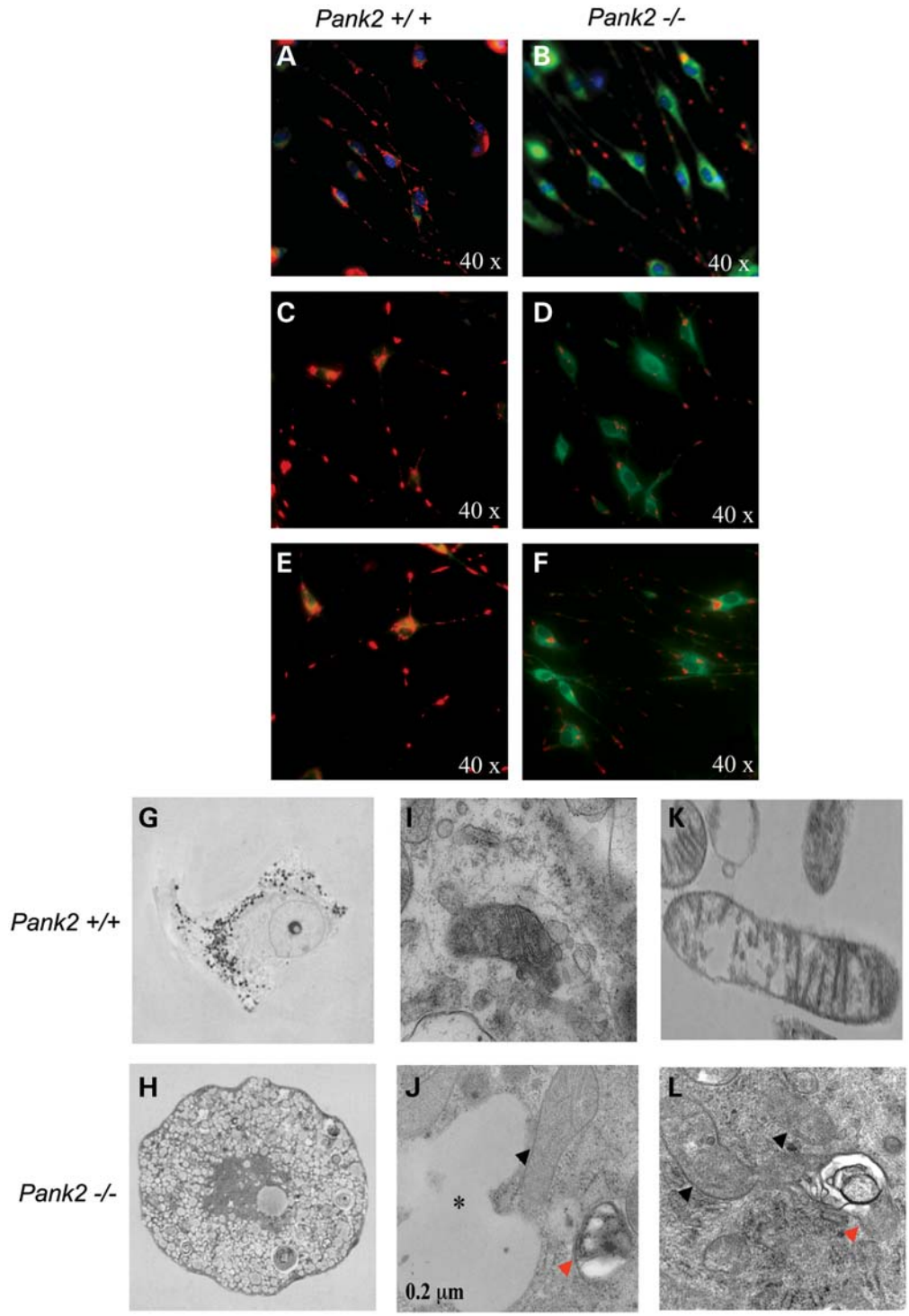

Figure 4. Membrane potential and electron microscopy in *Pank2*$^{+/+}$ and *Pank2*$^{-/-}$ neurons. (**A** and **B**) JC1 staining of neurons derived from hair bulge. (**C** and **D**) JC1 staining of neurons derived from sciatic nerve. (**E** and **F**) JC1 staining of neonatal neuron derived from hippocampus. Blue fluorescence indicates DAPI staining of nuclei. Green fluorescence indicates an alteration in mitochondrial $\Delta\Psi$; red fluorescence indicates the preservation of a normal mitochondrial $\Delta\Psi$. (**G** and **H**) Electron microscopy of neurons derived from sciatic nerve (semithin section Toluidin Blue). (**I**–**L**) Electron microscopy of neurons derived from sciatic nerve (ultrastructure uranyl acetate and lead citrate). Normal appearing mitochondria in *Pank2*$^{+/+}$ neurons (I–K) and few normal mitochondria in *Pank2*$^{-/-}$ neurons (black arrows in J–L); aberrant mitochondria with disrupted matrix and cristae (red arrows in J–L); lipid filled vesicle (asterisk in J).

our results in the nervous system of *Pank2*$^{-/-}$ mice in which mitochondria are severely damaged.

In search for mechanisms underlying the alteration of mitochondria, we found a reduced level of ATP in *Pank2*$^{-/-}$ mice. Interestingly, we found that state 3 activity, which represent the maximum respiration rate in the presence of ADP, is significantly decreased in mitochondria isolated from *Pank2*$^{-/-}$ mice. It is tempting to speculate that the reduction

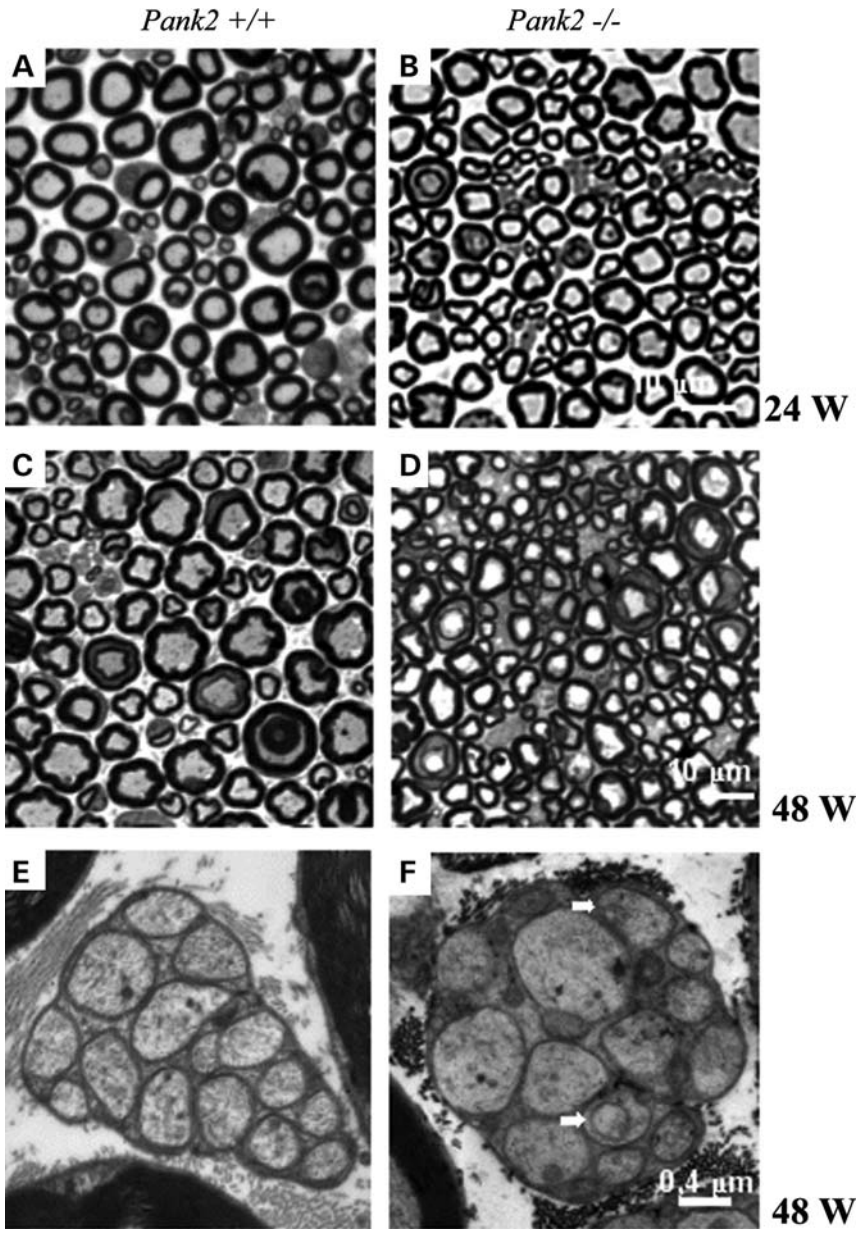

Figure 5. Evaluation of neurodegeneration of peripheral nervous systems with optic and electron microscopy. Sciatic nerve semithin section (Toluidin Blue) of (**A**) 24-week-old and (**C**) 48-week-old *Pank2*$^{+/+}$ mice; (**B**) 24-week-old and (**D**) 48-week-old *Pank2*$^{-/-}$ mice. Fibre density is not clearly different, whereas the axonal diameter seems to be reduced in *Pank2*$^{-/-}$. Electron micrographs of 48-week-old mice sciatic nerve in *Pank2*$^{+/+}$ mice (**E**) and *Pank2*$^{-/-}$ mice (**F**). No sign of un-myelinated fibre loss in the form of collagen pockets or denervated Schwann cells were evident; in *Pank2*$^{-/-}$ mice, some enlarged mitochondria were detected (arrows in F).

in the respiration could be attributable to the severe alteration of the cristae structure, which could prevent the respirasomes from remaining functionally active.

We also investigated the presence of oxidative damage in brains, but we did not find significant differences in oxidative damage at least in 6-month-old *Pank2*$^{-/-}$ mice. As demonstrated by other studies, mitochondrial membrane damage contributes to the pathogenesis of many neurodegenerative diseases (19,20).

Interestingly enough, a recent investigation of a KO mouse model for the *Pla2g6* gene, which is defective in a different but related form of NBIA, revealed the presence of collapsed mitochondria with degenerated inner membranes (21). *Pla2g6* gene encodes a group VIA calcium-independent phospholipase A2, an esterase that hydrolyzes the sn-2 ester bond in phospholipids to yield free fatty acids and lysophospholipids and which is involved in cardiolipin remodelling (22). Analysis of phospholipids and fatty acids revealed differences between KO and WT mice. The vulnerability of mitochondrial inner membranes in *Pla2g6* KO mice might be attributable to increased production of reactive oxygen species (ROS) (23) and a rich content of polyunsaturated fatty acids that can

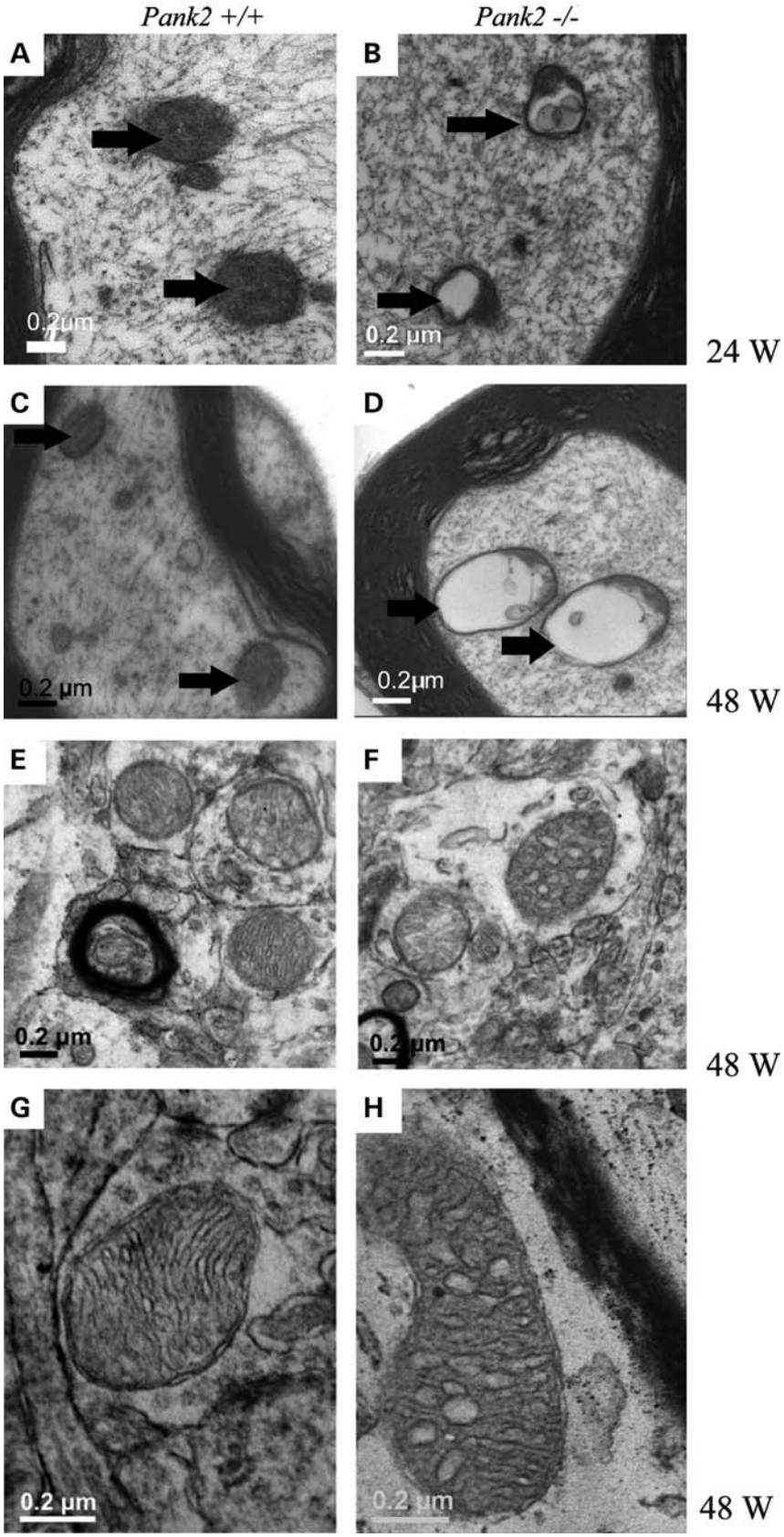

Figure 6. Electron microscopy of peripheral and CNS of 24- and 48-week-old animals. (**A**–**C**) Sciatic nerve of *Pank2*$^{+/+}$ mice show normal mitochondria (arrows). (**B**–**D**) Sciatic nerve of *Pank2*$^{-/-}$ mice show swollen mitochondria with altered cristae (arrows). (**E**–**G**) Basal ganglia derived from 48-week-old *Pank2*$^{+/+}$ mice show normally shaped mitochondria. (**F**–**H**) Basal ganglia derived from 48-week-old *Pank2*$^{-/-}$ mice show altered cristae and enlarged cisternae.

readily be peroxidized, such as linoleic acid in cardiolipin (22).

Alteration in cholesterol and lipid metabolism was also recently demonstrated by a metabolomics investigation in a group of PKAN patients (24). In this case, however, the alteration was mainly due to a defective synthesis and not, as in the case of PLA2G6, to the absence of a catabolic enzyme.

Irrespective of the anabolic (PANK2) or catabolic (PLA2G6) role of these two mitochondrial proteins, a common culprit in the pathogenesis of both neurodegenerative diseases could be an altered lipid metabolism (25). Further characterization of the lipid profile in *Pank2*$^{-/-}$ mice is in progress to understand if and how alteration of this metabolic pathway could be responsible for the observed mitochondrial membranes modifications.

We demonstrated insufficient energy production and severe mitochondrial dysfunction in the brain and peripheral nerve of *Pank2*$^{-/-}$ mice, without increased oxidative stress or signs of neurodegeneration. It is possible that mice can better tolerate alterations in bioenergetics metabolism without suffering any overt clinical manifestations because of the presence of compensatory mechanisms. Few examples of mouse models of mitochondrial disorders, which display a biochemical phenotype but do not present any clinical signs typical of the human pathology, are described in the literature (26,27).

Although we clearly demonstrated mitochondrial dysfunction in *Pank2*$^{-/-}$ mice, we remain uncertain why neither neurological signs typical of PKAN nor iron accumulation occur in mice. However, our findings suggest that there would be value in investigating bioenergetic competence and ultra-structural abnormalities of mitochondria in PKAN patients.

MATERIALS AND METHODS

Animals and diet

The use and care of animals followed the Italian Law D.L. 116/1992 and the EU directive 86/609/CEE. Animal studies were approved in accordance with guidelines of the Italian Ministry of Health: Project n. BT4/2011.

The JM129/SvJ–C57BL/6 *Pank2*$^{+/-}$ mice used in this study were the same as those generated in 2005 (7).

Animals were housed two or three per cage in a temperature-controlled (21°C) room with a 12 h light–dark cycle and ~60% relative humidity. Standard diet (DS, Mucedola, Italy) and water were given *ad libitum*.

Mitochondria isolation

Standard methods were used for the preparation of mitochondrial and post-mitochondrial fractions from mouse brain (28).

Brain was extracted and rinsed using cold homogenization medium AT [0.075 M sucrose, 0.225 M mannitol, 1 mM ethylene glycol tetraacetic acid (EGTA), 0.01% bovine serum albumin (BSA), pH 7.4]. The organ weighted was cut into small pieces and washed to remove blood and connective tissue. The brain was homogenized with 10–15 strokes using a Dounce-type glass homogenizer with a manually driven glass pestle, adding 5 ml of homogenization medium AT per gram of the starting material. The tissue was centrifuged at low speed (1000*g* for 5 min at 4°C) and the resulting supernatant was transferred to a clean tube and spin at high speed (9000*g* for 10 min at 4°C). The supernatant obtained from this centrifugation contained cytosol. To clean the mitochondrial pellet obtained, we resuspended it with 5 ml of medium AT, transferred to 1.5 ml Eppendorf tubes and washed to obtain a single pellet. The washed mitochondria were resuspended in the appropriate volume of MAITE medium (25 mM sucrose, 75 mM sorbitol, 100 mM KCl, 0.05 mM EDTA, 5 mM $MgCl_2$, 10 mM Tris–HCl, 10 mM H_3PO_4, pH 7.4). This fraction contained free mitochondria and synaptosomes.

Mitochondria fractionation

Isolated mitochondria were resuspended in 100 μl of potassium phosphate buffer [(PP) buffer, 20 mM, pH 7.8, KCl 150 mM] and sonicated 10 s for three times at 10 Amp. The suspension was centrifuged at 164000*g* for 30 min at 4°C. Supernatant (mitochondrial matrix and inter-membrane space) was collected, and pellet (mitochondrial membranes) was resuspended in 100 μl of PP buffer.

Isolation and fractionation of mitoplasts

Isolated mitochondria were resuspended in 100 μl of homogenisation medium A. After quantification of protein with Bradford method (Biorad), the sample was incubated for 5 min at 4°C with Digitonin (Fluka) at a final concentration of 0.18 mg for mg of protein. Digitonin was then diluted with 10 volumes of medium A and the sample was centrifuged at 12 000*g* for 10 min at 4°C. Supernatant (inter-membrane space) was collected, and pellet (mitoplasts) was resuspended in 100 μl of PP buffer.

Mitoplasts were then sonicated 10 s for three times at 10 Amp. The suspension was centrifuged at 164000*g* for 30 min at 4°C. Supernatant (mitochondrial matrix) was collected and pellet (mitochondrial inner membrane) was resuspended in 100 μl of PP buffer.

Western blot analysis

Thirty micrograms of proteins were used for each sample in denaturing sodium dodecyl sulphate–polyacrylamide gel electrophoresis (SDS–PAGE). Western blot analysis was performed as described (29), using the ECL-chemiluminescence kit (Amersham).

Antibodies

The following mouse monoclonal antibodies were used: anti-PANK2 (Origene) at 1:2000 dilution, anti-NADH dehydrogenase ubiquinone 1 alpha subcomplex subunit 9 (NDUFA9) (Invitrogen) at final concentration of 0.5 μg/ml and anti-Rieske (Invitrogen) at a final concentration of 2 μg/ml, anti-SDH-70 (succinate dehydrogenase, subunit 70 kDa) (Invitrogen) at 1:5000 dilution. An anti-ethylmalonic encephalopathy 1 rabbit polyclonal antibody was used at 1:2000 dilution (30). Secondary

anti-rabbit and anti-mouse antibodies were used at 1:10 000 and 1:7000 dilutions, respectively.

ATP and oxidative stress assays

ATPLite kit (PerkinElmer Life Sciences) was used to measure ATP levels according to manufacturer's instructions. This method is based on mono-oxygenation of luciferin, catalyzed by luciferase in the presence of Mg^{2+}, ATP and oxygen, resulting in a luminescent signal that is proportional to the ATP concentration.

Oxidized proteins were detected using the Oxyblot Protein Oxidation Detection Kit (Millipore) following the manufacturer's instructions. Brain extracts were homogenized in 20 mM Tris–HCl, pH 7, 50 mM dithiothreitol in the presence of anti-protease inhibitor cocktail tablet (Roche) and then derivatized to 2,4-dinitrophenylhydrazone. One microgram of proteins was loaded on 12% SDS–PAGE, blotted and incubated with an anti-DPN antibody. The bound activity was revealed by ECL Advance kit (Amersham).

Mitochondria membrane potential

Mitochondrial morphology was assessed after cell staining with 10 nM Mitotracker CMX-Red (Invitrogen) for 30 min at 37°C. Fluorescence was visualized with a digital imaging system using an inverted epifluorescence microscope with ×63/1.4 oil objective (Nikon, Japan). Images were captured with a back-illuminated Photometrics Cascade CCD camera system (Crisel) and analysed with Metamorph acquisition/analysis software. Different diffusion of the mitotraker in the neuron cytoplasm was quantified, calculating the parameter 'RawIntdens' of ImageJ software (http://rsbweb.nih.gov/ij/) that is the sum of the values of the pixels in selected areas. These data were calculated in 66 neurons (33 KO versus 33 WT) in three different experiments.

Detection of mitochondrial potential change was performed using JC1 (Sigma, CS0390) staining kit according to manufacturer' instructions.

Evaluation of bioenergetic profile

Measurements of oxygen consumption were performed on isolated mitochondria derived from mouse brain using an XF96 Extracellular Flux Analyser (Seahorse Bioscience).

To rapidly isolate mitochondria, brains were obtained from sacrificed mice and washed three times in ice-cold phosphate-buffered saline (PBS), than homogenized with 15 strokes in a glass-dounce homogenizer with 2 ml of hepes, EDTA, sucrose (HES)–0.2% BSA (HEPES 5 mM, EDTA 1 mM, sucrose 250 mM, BSA 0.2%, pH 7.4).

The homogenate was centrifuged for 10 min 2000 rpm (700*g*) at 4°C, and the supernatant was collected in a new tube, the pellet was resuspended in HES–0.2% BSA and centrifuged for 10 min 2000 rpm at 4°C.

The supernatant was collected and centrifuged for 15 min at 9000*g* and the supernatant was discarded; the pellet was resuspended in HES–0.2% BSA and centrifuged for 15 min 10 000 rpm and the supernatant was discarded.

The pellet containing mitochondria was resuspended in HES–0.2% BSA and total protein (mg/ml) was determined using Bradford Assay reagent (Bio-Rad).

As indicated by Rogers *et al.* (13), the WT and KO brain mitochondria were seeded in an XF 96-well cell culture microplate (Seahorse Bioscience) at a protein concentration of 8 μg/well in 50 μl of MAS-1 1× (70 mM sucrose, 220 mM mannitol, 10 mM KH_2PO_4, 5 mM $MgCl_2$, 2 mM HEPES, 1 mM EGTA and 0.2% (w/v) fatty acid-free BSA, pH 7.2) supplemented with succinate, malate, glutamate and pyruvate 5 mM. The plate was centrifuged 2000*g* for 5 min at 4°C, 130 μl of succinate, malate, glutamate and pyruvate 5 mM were added and incubated at 37°C without CO_2 for 30 min before starting the assay.

OCR was measured under basal condition (OCR-B), and after sequentially adding to each well 20 μl of ADP (OCR-ADP) and 22 μl of oligomycin (OCR-OL) to reach working concentrations of 4 mM and 2.5 μM respectively. OCR was also measured after addition of carbonyl cyanide 4-(trifluoromethoxy) phenylhydrazone (FCCP), to evaluate the maximal respiratory capacity.

The detailed protocol was as follows:

1′ Mixing
3′ Waiting
1′ Mixing
3′ Waiting

Basal OCR:

30″ Mixing
3′ Recording
1′ Mixing
3′ Recording
30″ Mixing

ADP addition through port A

1′ Mixing
3′ Recording
1′ Mixing
3′ Recording
1′ Mixing

Oligomycin addition through port B

30″ Mixing
3′ Recording
1′ Mixing
3′ Recording
1′ Mixing
3′ Recording

Statistics

For individual experiments, data obtained from $Pank2^{+/+}$ and $Pank2^{-/-}$ mitochondria were calculated as the mean of the replicates ± standard deviation (SD) and then compared with unpaired two-tailed Student's *t*-test. Although the measurements obtained from the replicates for each sample were relatively consistent in individual experiments, the values may vary in different experiments performed in different days. For this reason, we transformed each value of OCR-B,

OCR-ADP, OCR-O and OCR-F into standard (z) scores, in order to make the data of three different experiments comparable with each other and perform statistical analysis to the entire collection of experimental values. In practice, for each sample, the overall mean was subtracted from each measure, and the result was divided by the overall SD of the experiment. The resulting values indicate how many SD's separate a given observation from the reference value of the experiment.

Transformed data were then compared across samples and across experiments by unpaired two-tailed Student's t-test. Results with $P < 0.05$ were considered statistically significant.

Electron microscopy analysis

Sciatic nerves samples from 24- and 48-week-old *Pank2*$^{+/+}$ and *Pank2*$^{-/-}$ mice were surgically removed and fixed in glutaraledehyde 2.5% in phosphate buffer (pH = 7.4), post-fixed in aqueous solution of osmium tetroxide, dehydrated in acetone and embedded in epoxy resin (SPURR, EM Sciences). One-millimetre-thick sections were stained with Toluidine Blue.

For ultra-structural analysis, sections of 90 nm were collected on 200-mesh copper grids, positively stained with uranyl acetate and lead citrate, and then analysed by transmission electron microscope (EM109 Zeiss) to evaluate the presence of possible alterations in axonal morphology, cell membranes and mitochondria.

Sagittally spliced brains from 72-week-old *Pank2*$^{+/+}$ and *Pank2*$^{-/-}$ mice were fixed by immersion in 4% paraformaldehyde–PBS. After fixation, serial sagittal slides of ~1 mm thick were obtained. Selected areas of interest were sampled, post-fixed in osmium tetroxide and embedded in Epon epoxy resin. Thin sections (80–90 nm) were stained with uracyl acetate and lead citrate and examined with a CM10 Philips electron microscope.

Neurons derived from sciatic nerve were collected by gentle scraping and fixed in glutaraledehyde 2.5% in phosphate buffer (pH = 7.4). Cells pellet was treated for ultra-structural analyses as described above.

SUPPLEMENTARY MATERIAL

Supplementary Material is available at *HMG* online.

ACKNOWLEDGEMENTS

We would like to thank Sabrina Ravaglia, MD, University of Pavia, for helpful discussion about statistical analysis of z-scores and SIlvia Capra, Neurological Institute C. Besta, for technical support.

Conflict of Interest statement. None declared.

FUNDING

The financial support of Mariani Foundation of Milan (grant no. R-10-84 to V.T.) and Telethon GGP 11088 to V.T. and S.L. is gratefully acknowledged. S.H. and V.T. participate in the TIRCON consortium funded by the European Commission Seventh Framework Program (FP7/2007-2013, HEALTH-F2-2011) under Grant Agreement No. 277984. Funding to pay the Open Access publication charges for this article was provided by Fondazione Telethon, Italy.

REFERENCES

1. Spector, R. and Johanson, C.E. (2007) Vitamin transport and homeostasis in mammalian brain: focus on Vitamins B and E. *J. Neurochem.*, **103**, 425–438.
2. Daugherty, M., Polanuyer, B., Farrell, M., Scholle, M., Lykidis, A., de Crécy-Lagard, V. and Osterman, A. (2002) Complete reconstitution of the human coenzyme A biosynthetic pathway via comparative genomics. *J. Biol. Chem.*, **277**, 21431–21439.
3. Skrede, S. and Halvorsen, O. (1979) Mitochondrial biosynthesis of coenzyme A. *Biochem. Biophys. Res. Commun.*, **91**, 1536–1542.
4. Hörtnagel, K., Prokisch, H. and Meitinger, T. (2003) An isoform of hPANK2, deficient in pantothenate kinase-associated neurodegeneration, localizes to mitochondria. *Hum. Mol. Genet.*, **12**, 321–327.
5. Afshar, K., Gönczy, P., DiNardo, S. and Wasserman, S.A. (2001) Fumble encodes a pantothenate kinase homolog required for proper mitosis and meiosis in *Drosophila melanogaster*. *Genetics*, **157**, 1267–1276.
6. Zhou, B., Westaway, S.K., Levinson, B., Johnson, M.A., Gitschier, J. and Hayflick, S.J. (2001) A novel pantothenate kinase gene (PANK2) is defective in Hallervorden–Spatz syndrome. *Nat. Genet.*, **28**, 345–349.
7. Kuo, Y.M., Duncan, J.L., Westaway, S.K., Yang, H., Nune, G., Xu, E.Y., Hayflick, S.J. and Gitschier, J. (2005) Deficiency of pantothenate kinase 2 (Pank2) in mice leads to retinal degeneration and azoospermia. *Hum. Mol. Genet.*, **14**, 49–57.
8. Kuo, Y.M., Hayflick, S.J. and Gitschier, J. (2007) Deprivation of pantothenic acid elicits a movement disorder and azoospermia in a mouse model of pantothenate kinase-associated neurodegeneration. *J. Inherit. Metab. Dis.*, **30**, 310–317.
9. Johnson, M.A., Kuo, Y.M., Westaway, S.K., Parker, S.M., Ching, K.H., Gitschier, J. and Hayflick, S.J. (2004) Mitochondrial localization of human PANK2 and hypotheses of secondary iron accumulation in pantothenate kinase-associated neurodegeneration. *Ann. N. Y. Acad. Sci.*, **1012**, 282–298.
10. Leonardi, R., Zhang, Y.M., Lykidis, A., Rock, C.O. and Jackowski, S. (2007) Localization and regulation of mouse pantothenate kinase 2. *FEBS Lett.*, **581**, 4639–4644.
11. Brand, M.D. and Nicholls, D.G. (2011) Assessing mitochondrial dysfunction in cells. *Biochem. J.*, **435**, 297–312.
12. Invernizzi, F., D'Amato, I., Jensen, P.B., Ravaglia, S., Zeviani, M. and Tiranti, V. (2012) Microscale oxygraphy reveals OXPHOS impairment in MRC mutant cells. *Mitochondrion*, **12**, 328–335.
13. Rogers, G.W., Brand, M.D., Petrosyan, S., Ashok, D., Elorza, A.A., Ferrick, D.A. and Murphy, A.N. (2011) High throughput microplate respiratory measurements using minimal quantities of isolated mitochondria. *PLoS One*, **6**, e21746.
14. Buckman, J.F., Hernández, H., Kress, G.J., Votyakova, T.V., Pal, S. and Reynolds, I.J. (2001) MitoTracker labeling in primary neuronal and astrocytic cultures: influence of mitochondrial membrane potential and oxidants. *J. Neurosci. Methods*, **104**, 165–176.
15. Wittig, I. and Schägger, H. (2009) Supramolecular organization of ATP synthase and respiratory chain in mitochondrial membranes. *Biochim. Biophys. Acta*, **1787**, 672–680.
16. Acín-Pérez, R., Fernández-Silva, P., Peleato, M.L., Pérez-Martos, A. and Enriquez, J.A. (2008) Respiratory active mitochondrial supercomplexes. *Mol. Cell.*, **32**, 529–539.
17. Bosveld, F., Rana, A., van der Wouden, P.E., Lemstra, W., Ritsema, M., Kampinga, H.H. and Sibon, O.C. (2008) De novo CoA biosynthesis is required to maintain DNA integrity during development of the *Drosophila* nervous system. *Hum. Mol. Genet.*, **17**, 2058–2069.
18. Rana, A., Seinen, E., Siudeja, K., Muntendam, R., Srinivasan, B., van der Want, J.J., Hayflick, S., Reijngoud, D.J., Kayser, O. and Sibon, O.C. (2010) Pantethine rescues a *Drosophila* model for pantothenate kinase-associated neurodegeneration. *Proc. Natl Acad. Sci. USA*, **107**, 6988–6993.

19. Knott, A.B., Perkins, G., Schwarzenbacher, R. and Bossy-Wetzel, E. (2008) Mitochondrial fragmentation in neurodegeneration. *Nat. Rev. Neurosci.*, **9**, 505–518.
20. Lin, M.T. and Beal, M.F. (2006) Mitochondrial dysfunction and oxidative stress in neurodegenerative diseases. *Nature*, **443**, 787–795.
21. Beck, G., Sugiura, Y., Shinzawa, K., Kato, S., Setou, M., Tsujimoto, Y., Sakoda, S. and Sumi-Akamaru, H. (2011) Neuroaxonal dystrophy in calcium-independent phospholipase A2β deficiency results from insufficient remodeling and degeneration of mitochondrial and presynaptic membranes. *J. Neurosci.*, **31**, 11411–11420.
22. Zhao, Z., Zhang, X., Zhao, C., Choi, J., Shi, J., Song, K., Turk, J. and Ma, Z.A. (2010) Protection of pancreatic beta-cells by group VIA phospholipase A(2)-mediated repair of mitochondrial membrane peroxidation. *Endocrinology*, **151**, 3038–3048.
23. McBride, H.M., Neuspiel, M. and Wasiak, S. (2006) Mitochondria: more than just a powerhouse. *Curr. Biol.*, **16**, 551–560.
24. Leoni, V., Strittmatter, L., Zorzi, G., Zibordi, F., Dusi, S., Garavaglia, B., Venco, P., Caccia, C., Souza, A.L., Deik, A. *et al.* (2011) Metabolic consequences of mitochondrial coenzyme A deficiency in patients with PANK2 mutations. *Mol. Genet. Metab.*, **105**, 463–471.
25. Kotzbauer, P.T., Truax, A.C., Trojanowski, J.Q. and Lee, V.M. (2005) Altered neuronal mitochondrial coenzyme A synthesis in neurodegeneration with brain iron accumulation caused by abnormal processing, stability, and catalytic activity of mutant pantothenate kinase 2. *J. Neurosci.*, **25**, 689–698.
26. Viscomi, C., Spinazzola, A., Maggioni, M., Fernandez-Vizarra, E., Massa, V., Pagano, C., Vettor, R., Mora, M. and Zeviani, M. (2009) Early-onset liver mtDNA depletion and late-onset proteinuric nephropathy in Mpv17 knockout mice. *Hum. Mol. Genet.*, **18**, 12–26.
27. Dell'agnello, C., Leo, S., Agostino, A., Szabadkai, G., Tiveron, C., Zulian, A., Prelle, A., Roubertoux, P., Rizzuto, R. and Zeviani, M. (2007) Increased longevity and refractoriness to Ca(2+)-dependent neurodegeneration in Surf1 knockout mice. *Hum. Mol. Genet.*, **16**, 431–444.
28. Fernández-Vizarra, E., López-Pérez, M.J. and Enriquez, J.A. (2002) Isolation of biogenetically competent mitochondria from mammalian tissues and cultured cells. *Methods*, **26**, 292–297.
29. Tiranti, V., Galimberti, C., Nijtmans, L., Bovolenta, S., Perini, M.P. and Zeviani, M. (1999) Characterization of SURF-1 expression and Surf-1p function in normal and disease conditions. *Hum. Mol. Genet.*, **8**, 2533–2540.
30. Tiranti, V., D'Adamo, P., Briem, E., Ferrari, G., Mineri, R., Lamantea, E., Mandel, H., Balestri, P., Garcia-Silva, M.T., Vollmer, B. *et al.* (2004) Ethylmalonic encephalopathy is caused by mutations in ETHE1, a gene encoding a mitochondrial matrix protein. *Am. J. Hum. Genet.*, **74**, 239–252.